Chinese Chemical Letters 35 (2024) 108623

Contents lists available at ScienceDirect

Chinese Chemical Letters

journal homepage: www.elsevier.com/locate/cclet

Polyphenol-mediated interfacial deposition strategy for supported manganese oxide catalysts with excellent pollutant degradation performance

Dong Cheng[a], Youyou Feng[a], Bingxi Feng[a], Ke Wang[b], Guoxin Song[c], Gen Wang[b,*], Xiaoli Cheng[d], Yonghui Deng[c], Jing Wei[a,*]

[a] The Key Laboratory of Biomedical Information Engineering of Ministry of Education, State Key Lab of Transducer Technology, School of Life Science and Technology, Xi'an Jiaotong University, Xi'an 710049, China
[b] School of Environmental and Municipal Engineering, Xi'an University of Architecture and Technology, Xi'an 710055, China
[c] Department of Chemistry, State Key Laboratory of Molecular Engineering of Polymers, State Key Laboratory of Transducer Technology, Fudan University, Shanghai 200433, China
[d] Key Laboratory of Functional Inorganic Material Chemistry, Ministry of Education, School of Chemistry and Materials Science, Heilongjiang University, Harbin 150080, China

ARTICLE INFO

Article history:
Received 25 March 2023
Revised 22 May 2023
Accepted 29 May 2023
Available online 3 June 2023

Keywords:
Redox strategy
Manganese oxides
Fixed catalyst
Peroxymonosulfate
PPCPs

ABSTRACT

In persulfate-based advanced oxidation process (PS-AOPs), fixing nanosized metal oxide on processable substrates is highly desirable to avoid the aggregation and loss of nanocatalysts during the practical application. However, it is still challenging to develop a versatile strategy for the deposition of metal oxide nanocatalysts on various substrates with different physicochemical properties. Herein, polyphenols are utilized as a "molecular glue" and reductant to mediate the interfacial deposition of MnO_2 nanocatalysts on different substrates. MnO_2 nanocatalysts were *in-situ* grown on macroscope mineral substrates (*e.g.*, airstone) *via* an interfacial redox strategy between tannic acid (TA) and oxidized $KMnO_4$, and then employed as a fixed catalyst of peroxymonosulfate (PMS) activation for treating pharmaceutical and personal care products (PPCPs) in water. The fixed MnO_2 exhibited superior catalytic performance toward different PPCPS via a singlet oxygen ($^1O_2$)-dominated nonradical oxidation pathway. PPCPs in the secondary effluent of wastewater treatment plants could be effectively removed by a fixed-bed column of the fixed MnO_2 with long term stability. Redox cycle of Mn^{4+}/Mn^{3+} and surface hydroxyl group of the fixed MnO_2 was proved to be responsible for the activation of PMS. This work provides a new avenue for developing fixed metal oxides for sustainable water treatment.

Water contamination caused by pharmaceutical and personal care products (PPCPs) has become a serious environmental issue due to their great risk to ecosystem and public health [1–3]. Inefficient removal of PPCPS in municipal wastewater treatment plants (WWTPs) is one of the main reasons for the discharge of PPCPS [4,5]. As PPCPs cannot be effectively removed by conventional water treatment technologies like coagulation and sedimentation, more and more attention has been paid on advanced oxidation process (AOPs) for treating PPCPs [6,7]. In particular, catalytically activated peroxymonosulfate (PMS)-based AOPs has drawn increasing interest owing to the high oxidation capacity, mild operation condition and wide working pH range [8].

Transition metal oxides (such as Co_3O_4, CuO, NiO and MnO_2) has been extensively studied for PMS activation as they are highly active and natural abundance [9–12]. Among them, manganese oxides are more appealing due to the lower toxicity and rich chemical valence states [13,14]. Besides, metastable manganese intermediates can trigger a singlet oxygen ($^1O_2$) dominated non-radical oxidation process, which are able to selectively degrade target contaminants in complicated water matrices [15,16]. By now, various manganese oxides with different architectures, chemical states and crystal structures have been explored to active PMS for wastewater decontamination [17]. To maximize the catalytic efficiency, the manganese oxides were generally applied as a powdery catalyst during the treatment process [18,19]. When suspended in water,

* Corresponding authors.
E-mail addresses: wanggen@xauat.edu.cn (G. Wang), jingwei@xjtu.edu.cn (J. Wei).

https://doi.org/10.1016/j.cclet.2023.108623
1001-8417/

however, the powdery manganese oxides were readily to aggregate and lose, which greatly restricted their application in actual wastewater treatment [20]. Fixing metal oxides on monolithic substrates (such as minerals, metal foams and ceramic membranes) can effectively address the problem of catalyst loss or aggregation [20–23]. Moreover, the fixed metal oxides could be installed in reactors of different shapes, which greatly favored their practical application [24]. Metal oxides were conventionally fixed through a slurry coating method by using a polymer binder, but suffered from the negative effect of polymer binder on the catalytic performance [25]. Recently, other strategies (such as chemical vapor deposition, hydrothermal method and spin coating) have also been explored to fix metal oxide catalysts but limited by the complicated synthesis process and extensive energy input [26]. Therefore, developing a facile and cost-effective strategy to fix manganese oxides on monolithic substrates is highly essential and desirable for sustainable water treatment.

Recently, mussel-inspired chemistry has attracted intensive attentions due to its superior adhesive property on various substrates [27–29]. Specially, Caruso's groups developed a simple, rapid and versatile coating strategy to deposit metal-polyphenol complex on various films and particles [30–32]. This coating technique is powerful to deposit different kinds of metal species (*e.g.*, Fe^{2+}, Co^{2+}, Ni^{2+}, Mn^{2+}) and polyphenol ligands on various substrates. Furthermore, polyphenols (*e.g.*, tannic acid) not only show excellent adhesive property towards different interfaces, but also are one kind of reductant due to the abundant catechol groups in the molecular skeleton [33–35]. For example, tannic acid (TA) has been widely used as an antioxidant. It has also been used as a reductant for the synthesis of noble metal nanoparticles [36,37]. Therefore, when combining the adhesive and reductive property of polyphenol, it is possible to deposit different kinds of metal oxides on various substrates. Till now, there are very few reports on the deposition of metal oxide on various interfaces based on the polyphenol redox chemistry.

Herein, a polyphenol-mediated interfacial deposition strategy was developed to coat MnO_2 on airstone, which is a kind of inert, chemically stable and low-cost minerals. The obtained composites were employed for PMS activation for sustainable degradation of PCPPs in the secondary effluent of WWTPs. The preparation process included the deposition of polyphenols (*e.g.*, TA) on airstone substrates followed by interfacial redox reactions between TA molecules and $KMnO_4$. Kinetic studies and mechanism investigations on PCPPs degradation over the fixed MnO_2 were systematically studied using bis-phenol A (BPA) as a probe contaminant. Sustainable degradation of different kinds of PCPPs was explored *via* a flow-through reaction in a column reactor of the fixed MnO_2, which revealed superior catalytic performance and long-term stability.

TA is a typical plant polyphenol with abundant phenolic hydroxyl groups and possesses strong reductive capability [38,39]. Hence, TA molecules were used to react with oxidative $KMnO_4$. MnO_2 nanoparticles were obtained as indicated by the rapid color change of TA solution and scanning electron microscopy (SEM) image of the collected precipitate (Figs. S1 and S2 in Supporting information). During the synthesis, TA acted like a molecule glue and coated first on the surface of airstone substrates. Then the modified airstone was dispersed in $KMnO_4$ solution, in which surface-coated TA molecules reduced $KMnO_4$ to MnO_2 nanoparticles to form MnO_2 *in-situ* on the airstone. The color of the airstone substrates was turned from white to dark after the deposition process, revealing the successful fixing of MnO_2 (Fig. 1a).

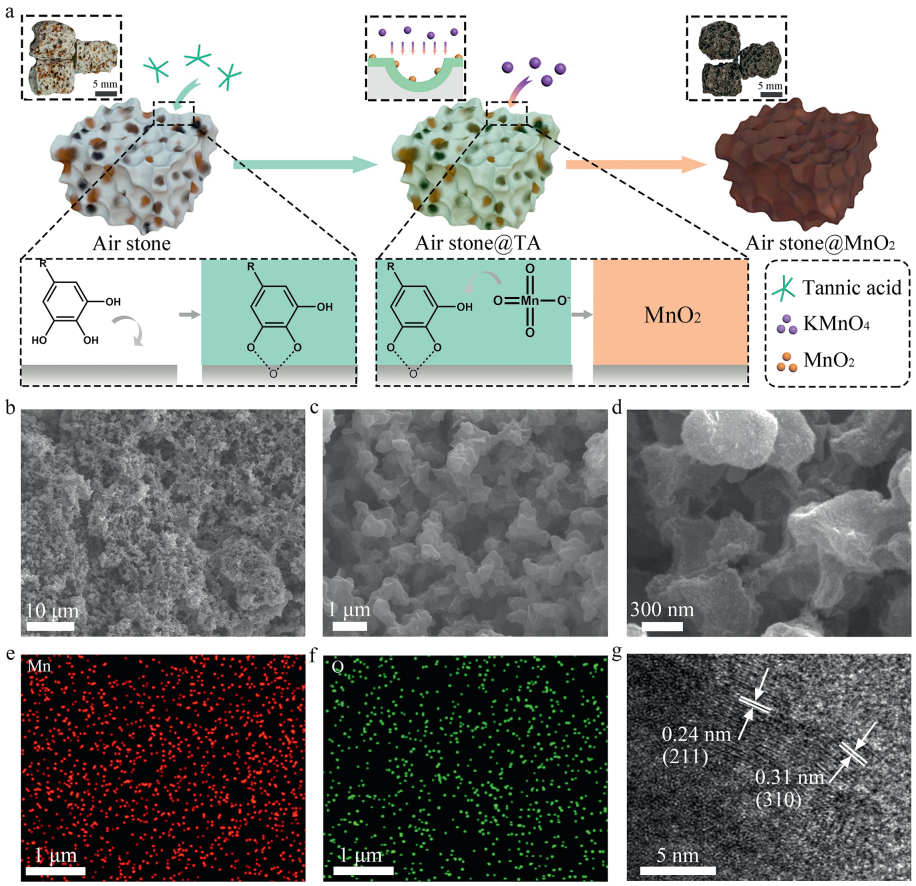

Fig. 1. (a) Schematic illustration for fixing MnO_2 on airstone substrates. (b) SEM image and (c, d) magnified SEM images of the fixed MnO_2. EDX elemental mapping of (e) Mn and (f) O, respectively. (g) HR-TEM image of the MnO_2.

SEM was applied to characterize the microstructure of the fixed MnO_2. As shown in Fig. 1b, MnO_2 nanoparticles with lose and porous structure were observed on the surface of airstone substrates whereas the pristine airstone displayed a smooth surface (Fig. S3 in Supporting information). The magnified SEM image further verified the porous structure (Figs. 1c and d). EDX mapping of the fixed MnO_2 revealed that Mn and O elements were homogeneously dispersed (Figs. 1e and f). HR-TEM image of the MnO_2 nanoparticles revealed low crystallinity (Fig. 1g). X-ray photoelectron spectroscopy (XPS) analysis and X-ray diffraction (XRD) pattern further confirmed low crystallinity of the fixed MnO_2 (Fig. S4 in Supporting information). The loading of MnO_2 on each gram of airstone substrate was determined to be ~0.07 mg according to the inductively coupled plasma (ICP) analysis.

Depositing metal oxides on processable substrates is highly required in different applications as it can overcome the aggregation problem of nanosized metal oxides [40,41]. The surface-independent adhesion property of TA allows *in-situ* deposition of metal oxides on diverse substrates with differernt shapes. As shown in Fig. 2, successful deposition of MnO_2 on different substrates was obtained, including metallic materials (*e.g.*, stainless steel, iron sheet and copper foil), non-metallic materials (*e.g.*, silicon wafer and glass flake) and polymer materials (*e.g.*, rubber sheet and plastic piece). There was insignificant difference between the SEM images of pristine substates and TA-modified substrates (Fig. S5 in Supporting information). However, FT-IR spectrum of the TA-modified airstone displayed new peaks of TA at 3327, 1715, 1611 and 1317 cm^{-1}, revealing the successful coating of TA (Fig. S6 in Supporting information). After reaction with $KMnO_4$, the characteristic peaks of TA were vanished revealing there was no residual of TA in the fixed MnO_2. The structure of deposited MnO_2 is tunable by regulating the reaction parameters. Sheet-like MnO_2 was formed at a low concentration of $KMnO_4$ (<1.0 mg/mL), while aggregated MnO_2 particles was obtained when excess amount of $KMnO_4$ (>1.0 mg/mL) was applied (Figs. 2c-f). N_2 sorption isotherms of the MnO_2 nanosheets exhibited type IV isotherms with a pore size centered at 5.1 nm (Fig. S7 in Supporting information), revealing a mesoporous structure. Aparting from MnO_2, other oxide (such as Cr_2O_3) was also successfully fixed on the airstone as indicated by the SEM image and EDS mapping (Fig. S8 in Supporting information), revealing the versatility of the proposed interfacial deposition strategy.

Batch experiments were performed to investigate the oxidation capacity of the fixed MnO_2/PMS system toward different organic contaminants. The removal of BPA in different reaction systems was compared firstly to study the degradation behavior of organic pollutant. As shown in Fig. 3a, only 8% of BPA was removed by PMS alone within 50 min, whereas complete removal of BPA was obtained in the fixed MnO_2/PMS system. The adsorption of BPA on the fixed MnO_2 was negligible and PMS catalyzed by airstone alone resulted in limited BPA removal (Fig. S9 in Supporting information). Besides, homogeneous catalysis of PMS by leached Mn^{2+} resulted in 20% removal of BPA. It indicated that the degradation of organic pollutant in the fixed MnO_2/PMS system mainly occurred *via* heterogeneous reactions [42]. The degradation of BPA followed first-order kinetic model with a rate constant of 0.1 min^{-1} ($R^2 = 0.98$) (Fig. 3a, inset), which was comparable with those of reported Mn-base metal oxides under similar reaction conditions (Table S1 in Supporting information). Interestingly, the degradation of BPA by 3.0 g of airstone with MnO_2 (corresponding to ~0.2 mg of pristine MnO_2) was much faster than that over 0.2 mg of powdery MnO_2 (Fig. S10 in Supporting information). The enhanced PMS activation efficiency clearly manifested the advantage of the fixed MnO_2, which relieved the aggregation problem of nanoparticles and thus afforded highly exposure of active sites. Besides, the structure of the fixed MnO_2 provided open diffusion channels and efficient mass transport of PMS and organic pollutant, which also contributed to the enhanced removal of BPA [43].

Apart from the endocrine disrupting chemicals (*e.g.*, BPA), the fixed MnO_2/PMS system was also effective toward a wide spectrum of PCPPs including pharmaceuticals (*e.g.*, acetaminophen, AAP), antibiotics (*e.g.*, sulfamethoxazole, SMX) and organic dyes (*e.g.*, methyl blue, MB). As shown in Fig. 3b, effective removal of AAP and MB was observed under the same reaction condition. Other organics like sulfamethoxazole (SMX), ibuprofen (IBU) and

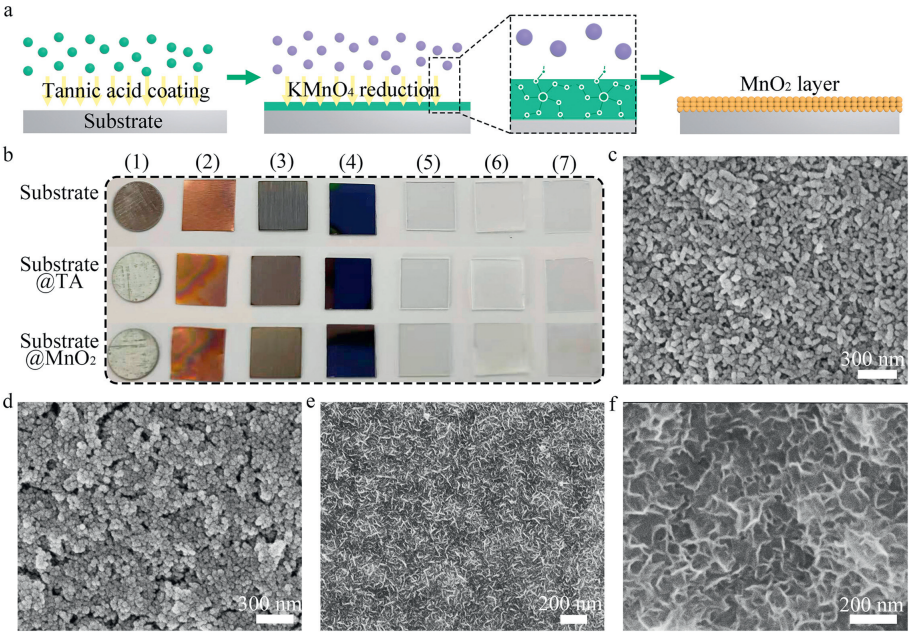

Fig. 2. (a) Schematic illustration for *in-situ* deposition of MnO_2 on different substrates. (b) Optical images of the substrates at different deposition stages: (1) iron sheet, (2) copper foil, (3) stainless steel sheet, (4) silicon wafer, (5) plastic piece, (6) rubber sheet and (7) glass flake. SEM images of MnO_2 nanoparticles or nanosheets deposited on (c) iron sheet, (d) copper foil, (e) stainless steel sheet and (f) silicon wafer surface.

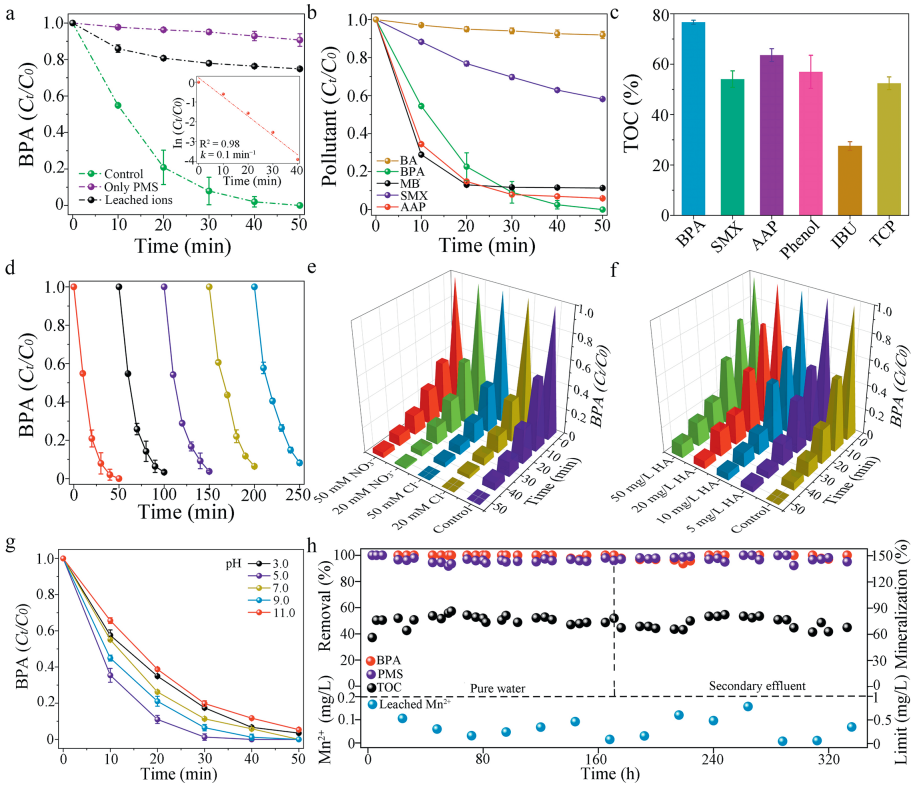

Fig. 3. (a) Degradation of BPA in different reaction systems. (b) Degradation of different PPCPs in the fixed MnO_2/PMS system. (c) TOC removal for different PPCPs. (d) Stability of the fixed MnO_2 in consecutive runs. The influence of (e) Cl^- and NO_3^- and (f) humic acid on the degradation of BPA. (g) Degradation of BPA in the pH range from 3 to 11. (h) Continuous degradation of BPA in pure water and actual secondary effluent of WWPTs in a fixed-bed column of the fixed MnO_2.

trichlorophenol (TCP) could also be degraded although a longer time was required (Fig. S11 in Supporting information). However, benzoic acid (BA) with electron-deficient groups could hardly be degraded under the same reaction condition, revealing the selective oxidation property of the fixed MnO_2 + PMS system. The kinetic rate for AAP, SMX and MB was determined to be 0.09, 0.01 and 0.1 min^{-1}, respectively (Fig. S12 in Supporting information). TOC removal of BPA, AAP, SMX, IBU, TCP and phenol was measured to be 77%, 64%, 54%, 28%, 52% and 57%, respectively (Fig. 3c), revealing PPCPs could be highly mineralized during the catalysis process. Besides, the fixed MnO_2 exhibited superior stability and reusability in PMS activation. The removal efficiency of BPA was still as high as 92% after 5 cycle runs (Fig. 3d). The excellent stability should be partly ascribed to the low leaching of Mn^{2+} (Fig. S13 in Supporting information). On the other hand, the MnO_2 was *in-situ* grown on airstone enabling strong adhesive of MnO_2 nanoparticles on the substrate, which also contributed to the excellent stability. The stability of the fixed MnO_2 was much higher than MnO_2 powder (Fig. S14 in Supporting information). Additionally, the catalytic activity of the fixed MnO_2 could be totally recovered *via* a facile calcination (Fig. S15 in Supporting information). The facile synthesis process, superior catalytic activity, excellent stability and simple regeneration strategy endowed the fixed MnO_2 promising potential for PCPPS treatment. Fixing nanosized catalyst on processable substrates enables additional advantages of easy installation in reactors and promising potential for practical application. Herein, aiming to explore the application potential, the performance of the fixed MnO_2 for treating PPCPs in the secondary effluent of WWTPs was investigated. Considering the complicated components of the secondary effluent and their possible quenching toward reactive oxygen species, the degradation of BPA in the presence of ubiquitous inorganic ions and natural organic matters (NOMs) was investigated first.

As shown in Fig. 3e, the addition of Cl^- and NO_3^- hardly inhibited the degradation of BPA even when a high concentration of 50 mmol/L was applied. Other inorganic ions (*e.g.*, SO_4^{2-} and CO_3^{2-}) of high concentrations also exhibited negligible influence on BPA removal (Fig. S16 in Supporting information). The good resistance toward inorganic ions was ascribed to the $^1O_2$-dominated nonradical oxidation mechanism (discussed later), which was moderate oxidative and less reactive with Cl^-, SO_4^{2-}, NO_3^- and CO_3^{2-}. Humic acid (HA) with a concentration from 5 mg/L to 50 mg/L showed insignificant influence on BPA removal as well (Fig. 3f), revealing the fixed MnO_2/PMS system also restricted to NOMs. Besides, the fixed MnO_2 had a wide working pH range (Fig. 3g). In comparison to the neutral condition, efficient removal of BPA was also obtained in acidic (pH 3, 5) and alkaline condition (pH 9, 11) with a slight decrease in kinetic rates. The fixed MnO_2 was then employed to build a fixed-bed column reactor to treat PCPPs in the secondary effluent *via* a continuous flow-through reaction. The long-term stability of the column reactor was firstly studied by continuously degrading BPA in ultra-pure water. As shown in Fig. 3h, BPA was completely removed in the first one week with a high mineralization efficiency (TOC removal was ~70%), revealing a superior stability of the fixed MnO_2. Then the ultra-pure water was replaced by secondary effluent of WWTP to explore the removal of BPA in actual wastewater. The removal efficiency of BPA was slightly decreased by ~3% probably due to the coverage of active sites by the background surroundings like NOMs [44]. Nevertheless, no further decline of BPA removal was observed and TOC was stably removed as well during one week of continuous reaction. Meanwhile, PMS was completely decomposed during the continuous run. The superior performance and excellent stability should be ascribed to the nonradical oxidation mechanism which was restricted to inorganic ions and NOMs. Moreover, the leaching of Mn^{2+} was low and met the requirement of the Environmen-

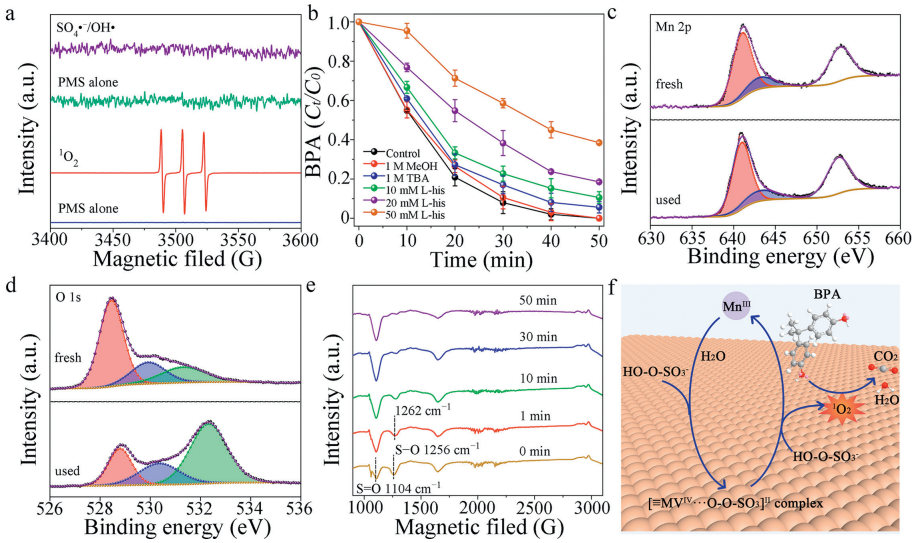

Fig. 4. (a) Detection of $SO_4^{\bullet-}$, $OH^{\bullet}$ and $^1O_2$ *via* EPR tests. (b) Quenching effect of MeOH, TBA and L-His on the degradation of BPA. (c) XPS spectra for Mn 2p and (d) O 1s before and after the catalysis reaction. (e) ATR-FTIR spectra for MnO_2/PMS at different times. (f) Schema for PMS activation and BPA degradation over the fixed MnO_2.

tal Quality Standards for Surface Water in China (EQSSW, GB3838–2002).

Both radical (*e.g.*, $OH^{\bullet}$ and $SO_4^{\bullet-}$) and nonradical oxidation (*e.g.*, $^1O_2$) have been proposed for organics degradation in PMS activation [13]. Herein, electron paramagnetic resonance (EPR) tests and chemical quenching experiments were performed to investigate the mechanism of PPCPs degradation. As shown in Fig. 4a, neither $SO_4^{\bullet-}$ nor $OH^{\bullet}$ was detected when 5,5-dimethyl-1-pyrroline *N*-oxide (DMPO) was used as the spin trapping agent, indicating that no radicals were produced during the activation of PMS [14,17,45]. Chemical quenching experiments using methanol (MeOH) and *tert*-buty alcohol (TBA) showed that the degradation of BPA was not influenced even when the concentration of scavengers was as high as 1000 mmol/L. Besides, negligible degradation of benzoic acid (BA, a typical probe for radicals) was observed in the fixed MnO_2/PMS system, further revealing the absence of radicals in organics degradation [46]. When 2,2,6,6-tetramethyl-4-piperidone (TEMP) was used as the trapping agent, however, characteristic singles of TEMP-$^1O_2$ adducts was observed. Furthermore, the removal of BPA was strongly inhibited by introducing L-histidine (L-His, a typical chemical probe for $^1O_2$). For example, the removal efficiency of BPA decreased by 80% when 50 mmol/L of L-His-was presented (Fig. 4b). It indicated that the degradation of PPCPs in the fixed MnO_2/PMS system followed a $^1O_2$-dominated nonradical oxidation pathway [47,48]. Chemical quenching experiments by benzoquinone (BQ, a scavenger for $O_2^{\bullet-}$) revealed that the degradation of BPA was strongly inhibited after the introduction of BQ (Fig. S17 in Supporting information), indicating the $^1O_2$ was originated from $O_2^{\bullet-}$ ($2O_2^{\bullet-} + H_2O_2 \rightarrow {}^1O_2 + H_2O_2 + 2OH^-$) [22,23]. The variation of chemical states of Mn and O was analyzed to explore the mechanism of PMS activation over the fixed MnO_2. After the catalysis reaction, the content of Mn^{4+} (643.2 eV) was decreased from 82.5% to 75.1% while the percentage of Mn^{3+} (641.1 eV) was increased from 17.5% to 24.9% (Fig. 4c). It indicated that the redox cycle of Mn^{4+}/Mn^{3+} induced the activation of PMS activation [49,50]. XPS spectra of O 1s for used MnO_2 showed that the percentage of surface oxygen was declined in comparison to that in the fresh MnO_2 (Fig. 4d). In PMS activation, H_2O molecules would be adsorbed on metal oxides surface and dissociated to form ≡Mn(IV)···OH and then participated in the subsequent metal oxide redox reaction [51]. *In-situ* attenuated total reflectance Fourier transform infrared spectroscopy (ATR-FTIR) was performed to further explore the activation process (Fig. 4e). For PMS alone, stretching vibration for S-O bond of SO_4^{2-} and HSO_5^- was displayed at 1104 and 1256 cm^{-1}, respectively. When contacted with the MnO_2, the S-O bond of HSO_5^- was blue-shifted by 6 cm^{-1}, suggesting the formation of chemical bond between MnO_2 and HSO_5^- [22,52]. Moreover, the peak intensity of the S-O decreased gradually upon increasing the reaction time, indicating continuous decomposition of PMS molecules on the surface of MnO_2. The results revealed that PMS was covalently bonded first with the MnO_2, resulting in the formation of ≡Mn(IV)···O–O-SO_3 complex on the surface (Eq. 1) (Fig. 4f). Then the complex reacted with another PMS molecule to produce $^1O_2$ and participated into the degradation of micropollutants (Eqs. 2 and 3).

$$[\equiv Mn(IV)\cdots OH]^{III} + HO\text{–}O\text{-}SO_3^- \rightarrow [\equiv Mn(IV)\cdots O\text{–}O\text{-}SO_3]^{II} + H_2O \quad (1)$$

$$2[\equiv Mn(IV)\cdots O\text{–}O\text{-}SO_3]^{II} + HO\text{–}O\text{-}SO_3^- + H_2O \rightarrow 2[\equiv Mn(III)\cdots O\text{–}O\text{-}SO_3]^{II} + 2{}^1O_2 + 5H^+ + 3SO_4^{2-} + H_2O_2 \quad (2)$$

$$^1O_2 + PPCPs \rightarrow \text{intermediates}/CO_2 + H_2O \quad (3)$$

In summary, MnO_2 was successfully fixed on airstone substrates *via in-situ* interfacial redox reactions between TA and $KMnO_4$. Fixing MnO_2 on the monolithic substrates allowed highly exposure of active sites and superior stability, and thus enabled superior catalytic performance toward PMS activation and PPCPs degradation with long-term stability. The degradation of PPCPs followed a $^1O_2$-donminated nonradical oxidation pathway with strong anti-interference ability toward inorganic ions and natural organic matters. The fixed MnO_2 could be installed in a column reactor for sustainable degradation of a wide spread of PPCPs in the secondary effluent of WWPTs. This work provided a reliable strategy for developing recoverable metal oxides with novel structures for sustainable water treatment.

Declaration of competing interest

The authors declare that they have no known competing financial interests or personal relationships that could have appeared to influence the work reported in this paper.

Acknowledgments

This work was financially supported by the National Key Research and Development Program (No. 2022YFE0100400), National Natural Science Foundation of China (No. 21701130), Key Basic Research Program of Science and Technology Commission of Shanghai Municipality (No. 20JC1415300), State Key Laboratory of Transducer Technology of China (No. SKT2207) and Key Research and Development Program of Shaanxi (No. 2021GY-225).

Supplementary materials

Supplementary material associated with this article can be found, in the online version, at doi:10.1016/j.cclet.2023.108623.

References

[1] J.L. Liu, M.H. Wong, Environ. Int. 59 (2013) 208–224.
[2] M.K. Shahid, A. Kashif, A. Fuwad, Y. Choi, Coord. Chem. Rev. 442 (2021) 213993.
[3] M. Narayanan, M. El-Sheekh, Y. Ma, et al., Environ. Pollut. 300 (2022) 118922.
[4] N.H. Tran, M. Reinhard, K.Y. Gin, Water Res. 133 (2018) 182–207.
[5] H.B. Quesada, A.T.A. Baptista, L.F. Cusioli, et al., Chemosphere 222 (2019) 766–780.
[6] R.Y. Krishnan, S. Manikandan, R. Subbaiya, et al., Environ. Technol. Innov. 23 (2021) 101757.
[7] A. Kujawska, U. Kiełkowska, A. Atisha, et al., Sep. Purif. Technol. 290 (2022) 120797.
[8] T. Liu, K. Cui, C.X. Li, et al., Chemosphere 311 (2023) 137084.
[9] W. Li, X. He, B. Li, et al., Appl. Catal. B: Environ. 305 (2022) 121019.
[10] S. Wang, S. Gao, J. Tian, et al., J. Hazard. Mater. 387 (2020) 121995.
[11] G. Wang, K. Wang, Z. Liu, et al., Appl. Catal. B: Environ. 325 (2023) 122359.
[12] R. Yang, Y. Fan, R. Ye, et al., Adv. Mater. 33 (2021) 2004862.
[13] M. Kohantorabi, G. Moussavi, S. Giannakis, Chem. Eng. J. 411 (2021) 127597.
[14] Y. Liu, J. Luo, L. Tang, et al., ACS Catal. 10 (2020) 14857–14870.
[15] Y. Yang, P. Zhang, K. Hu, et al., Appl. Catal. B: Environ. 315 (2022) 121593.
[16] L. Wang, J. Jiang, S.Y. Pang, et al., Chem. Eng. J. 352 (2018) 1004–2013.
[17] Y. Yang, P. Zhang, K. Hu, et al., Appl. Catal. B: Environ. 286 (2021) 119903.
[18] F. Pan, H. Ji, P. Du, et al., J. Hazard. Mater. 402 (2021) 123779.
[19] Y. Liu, R. Qu, X. Li, et al., J. Colloid Interface Sci. 579 (2020) 412–424.
[20] F. Ghanbari, M. Moradi, Chem. Eng. J. 310 (2017) 41–62.
[21] X. Dong, B. Ren, X. Zhang, et al., Appl. Catal. B: Environ. 272 (2020) 118971.
[22] X. Dong, X. Duan, Z. Sun, et al., Appl. Catal. B: Environ. 261 (2020) 118214.
[23] G. Wang, Y. Zhang, L. Ge, et al., J. Hazard. Mater. 429 (2022) 128282.
[24] G. Wang, L. Ge, Z. Liu, et al., Chem. Eng. J. 431 (2022) 134026.
[25] D. Chen, Q. Wang, R. Wang, et al., J. Mater. Chem. A 3 (2015) 10158–10173.
[26] S. Mathur, T. Ruegamer, N. Donia, J. Nanosci. Nanotechnol. 8 (2008) 2597–2603.
[27] Y. Liu, K. Ai, L. Lu, Chem. Rev. 114 (2014) 5057–5115.
[28] J. Saiz-Poseu, J. Mancebo-Aracil, F. Nador, et al., Angew. Chem. Int. Ed. 58 (2019) 696–714.
[29] E. Filippidi, T.R. Cristiani, C.D. Eisenbach, et al., Science 358 (2017) 502–505.
[30] H. Ejima, J.J. Richardson, K. Liang, et al., Science 341 (2013) 154–157.
[31] H. Geng, Q.Z. Zhong, J. Li, et al., Chem. Rev. 122 (2022) 11432–11473.
[32] J. Zhou, Z. Lin, M. Penna, et al., Nat. Commun. 11 (2020) 4804.
[33] J. Guo, Y. Ping, H. Ejima, et al., Angew. Chem. Int. Ed. 53 (2014) 5546–5551.
[34] J. Qin, G. Liang, B. Feng, et al., Chin. Chem. Lett. 32 (2021) 842–848.
[35] S. Quideau, D. Deffieux, C. Douat-Casassus, et al., Angew. Chem. Int. Ed. 50 (2011) 586–621.
[36] Y. Feng, P. Li, J. Wei, Coord. Chem. Rev. 468 (2022) 214649.
[37] B. Feng, Y. Feng, Y. Li, et al., ACS Sens. 7 (2022) 3963–3972.
[38] J. Wei, G. Wang, F. Chen, et al., Angew. Chem. Int. Ed. 57 (2018) 9838–9843.
[39] G. Wang, J. Qin, X. Zhou, et al., Adv. Funct. Mater. 28 (2018) 1806144.
[40] X. Dong, Z. Chen, A. Tang, et al., Adv. Funct. Mater. 32 (2022) 2111565.
[41] L. Zhu, J. Ji, J. Liu, et al., Angew. Chem. Int. Ed. 59 (2020) 13968–13976.
[42] C. Huang, Y. Wang, M. Gong, et al., Sep. Purif. Technol. 230 (2020) 115877.
[43] J. Huang, Y. Dai, K. Singewald, et al., Chem. Eng. J. 370 (2019) 906–915.
[44] Q.Z. Zhong, S. Li, J. Chen, et al., Angew. Chem. Int. Ed. 58 (2019) 12563–12568.
[45] J. Ji, Q. Yan, P. Yin, et al., Angew. Chem. Int. Ed. 60 (2021) 2903–2908.
[46] S. Zhu, X. Li, J. Kang, et al., Environ. Sci. Technol. 53 (2019) 307–315.
[47] X. Li, J. Wang, X. Duan, et al., ACS Catal. 11 (2021) 4848–4861.
[48] P. Shao, J. Tian, F. Yang, et al., Adv. Funct. Mater. 28 (2018) 1705295.
[49] G.X. Huang, C.Y. Wang, C.W. Yang, et al., Environ. Sci. Technol. 51 (2017) 12611–12618.
[50] J. Huang, S. Zhong, Y. Dai, et al., Environ. Sci. Technol. 52 (2018) 11309–11318.
[51] Z. Chen, S. Bi, G. Zhao, et al., Sci. Total Environ. 711 (2020) 134715.
[52] S. Yang, S. Xu, J. Tong, et al., Appl. Catal. B: Environ. 295 (2021) 120291.